Synthesis of PdS/ZnS–CdS-type photocatalysts using ZnS as sulphide source

Radu BANICA, Petrica LINUL, Cristina MOSOARCA[*]
Renewable Energy Laboratory, National Institute for Research and Development in Electrochemistry
and Condensed Matter, Timisoara, Romania

Abstract: In this work, a new method for the growth of large CdS crystals into PdS/ZnS–CdS-type photocatalysts is presented. In order to accomplish this, in the first stage zinc sulphide was synthesised and hydrothermally crystallised. In the second stage, after PdS decoration, the recrystallised zinc sulphide was utilised as sulphur source for the synthesis of PdS/ZnS–CdS-type photocatalysts. The photocatalysts were characterised by X-ray diffraction, transmission electron microscopy, energy dispersive X-ray spectroscopy, and diffuse reflectance spectroscopy. In the third stage magnetic polymer supports were manufactured and loaded with photocatalyst. Finally photocatalysis experiments under blue light illumination were conducted for the hydrogen evolution reaction in the presence of sulphite and sulphide ions on both suspension and polymer supported photocatalysts. The photocatalysts' efficiency increased by about 70% along with the PdS quantity increase from 0.11% to 0.89%. The use of magnetic polymer may be a solution for reducing the costs necessary to maintain the photocatalysts in suspension.

Key words: Water splitting, CdS photocatalyst, supported photocatalyst

1. Introduction

Hydrogen evolution from water using sunlight by photocatalysis is a topic of great interest.[1−5] CdS is the most efficient photocatalyst that absorbs the visible light for the water splitting reaction. However, CdS–ZnS-type photocatalyst mixtures have a higher photocatalytic efficiency in the water splitting reaction than the CdS and ZnS pure compounds.[1,6] Meanwhile, for achieving maximum photocatalyst efficiency it is necessary to have intimate contact between CdS and ZnS nanoparticles to ensure the injection of photogenerated carriers between semiconductor particles. The intimate contact was obtained by H_2S treatment of the polymer bands soaked in zinc acetate and cadmium acetate, by coprecipitation of metals with Na_2S, from reverse micelles, or by a combined hydrothermal-precipitation method.[1,6−8]

A CdS:ZnS molar ratio between 1:1 and 2:1 yields the most efficient photocatalysts.[1,6] Utilising photocatalysts supported on polymer bands leads to a lower cost photocatalytic process due to the fact that stirring is not necessary for maintaining the photocatalyst in suspension. To prevent the sulphur ions' oxidation from the CdS structure (photocatalyst photocorrosion), the photocatalysis reactions must be conducted in the presence of S^{2-} and SO_3^{2-} ions, which behave like a hole-scavenger.[6,9] Even in these conditions, after photocatalysis times ranging from a few hours to tens of hours, the photocatalyst activity begins to drop.[10−13] By a novel two-step thermal sulphuration method highly stable CdS can be obtained.[9] The coverage of ZnO nanobars by a window layer of CdS can be obtained.[9]
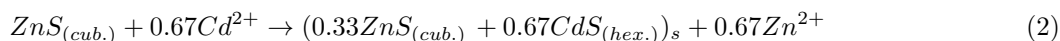
---

*Correspondence: mosoarca.c@gmail.com

In order to facilitate electron transfer from the CdS conduction band to the water molecule, CdS is often decorated with noble metals like Pt,[14,15] Pd,[14−17] Ru,[14,18,19] and Rh[14,20], which increases the photocatalyst price. Out of these metals, palladium has the lowest price. After we showed in a previous study that the efficiency of the obtained photocatalysts for the water splitting reaction is increasing with the ZnS precursor crystallinity increase in ZnS:CdS mixtures.[17] In this study we focused on obtaining ZnS:CdS mixtures by reactive dissolution of crystallised ZnS accompanying the charging of semiconductors with different quantities of PdS. In some cases magnetic polymeric bands were manufactured, loaded with photocatalyst, and magnetically fixed inside the photoreactor to avoid the use of stirring for maintaining the photocatalyst in suspension.

2. Results and discussion

When adding the $PdCl_2$ solution to the ZnS suspension, due to the reduced solubility at room temperature $(K_{sp\,PdS} = 2 \times 10^{-37}$ mol^2/L^2 vs. 10^{-23} mol^2/L^2 for β-ZnS),[17,21,22] the Pd^{2+} ions replace the Zn^{2+} ions on the surface of ZnS nanoparticles as shown in reaction r1. The Ksp values for the ZnS and CdS compounds at room temperature are not so different from each other (cca. 10^{-23} mol^2/L^2 for β-ZnS vs. cca. 10^{-27} mol^2/L^2 for CdS). For this reason when adding the cadmium salt on the white ZnS suspension, the yellow CdS formation at room temperature it is not noticeable. The ion exchange rate between Zn^{2+} and Cd^{2+}, as shown in reaction r2, increases with the temperature increase.

The reactions that take place are as follows:

$$ZnS + Pd^{2+} \rightarrow PdS + Zn^{2+} \tag{1}$$

$$ZnS_{(cub.)} + 0.67Cd^{2+} \rightarrow (0.33ZnS_{(cub.)} + 0.67CdS_{(hex.)})_s + 0.67Zn^{2+} \tag{2}$$

From the XRD data, as shown in Figure 1, it can be observed that the phase majority in the sample is represented by hexagonal cadmium sulphide (ICCD PDF no 00-089-2944) grown preferentially along the direction (101). Cubic ZnS is also present (ICCD PDF no 00-001-0792). Surprisingly, the Pd^{2+} presence in the system influences the CdS growth, the intensity of the XRD maxima corresponding to the planes with Miller indices (101–105), indicated by arrows, increasing with the increase in PdS quantity in the system. The Pd^{2+} ions' concentration in the hydrothermal system is given by the PdS solubility at a temperature of 200 °C. Due to the extremely low solubility of PdS, during the hydrothermal process the solution is saturated with this substance regardless of the $PdCl_2$ quantity added, which varies between 1.20 and 10.24 mg.

Thus the Pd^{2+} concentration in the H_2S containing system at 200 °C is constant, being in the range of ppb,[22] meaning with about 4 up to 5 orders of magnitude lower than the concentration that could have been reached by adding $PdCl_2$ in the absence of H_2S. However, at all concentrations, PdS can cause the heterogeneous nucleation of CdS, facilitating the crystal growth in the <101>direction.

The XRD spectra do not show the displacement of diffraction peaks of CdS for different concentrations of $PdCl_2$ added which suggests that the $PdCl_2$ added quantity does not influence the doping degree of CdS with Pd^{2+}. This observation sustains the fact that during the hydrothermal process, the palladium concentration is constant. The DSR spectra, as shown in Figure 2, confirms this hypothesis; the decrease in reflectance values due to the band to band transition is made at the same wavelength value for all the samples.

The band gap (Eg) value for the photocatalysts was calculated by expressing $(K-ME)^2 = f(E)$, where K-M is the Kubelka function value and E the energy of incident photons expressed in electron-volts and extrapolating
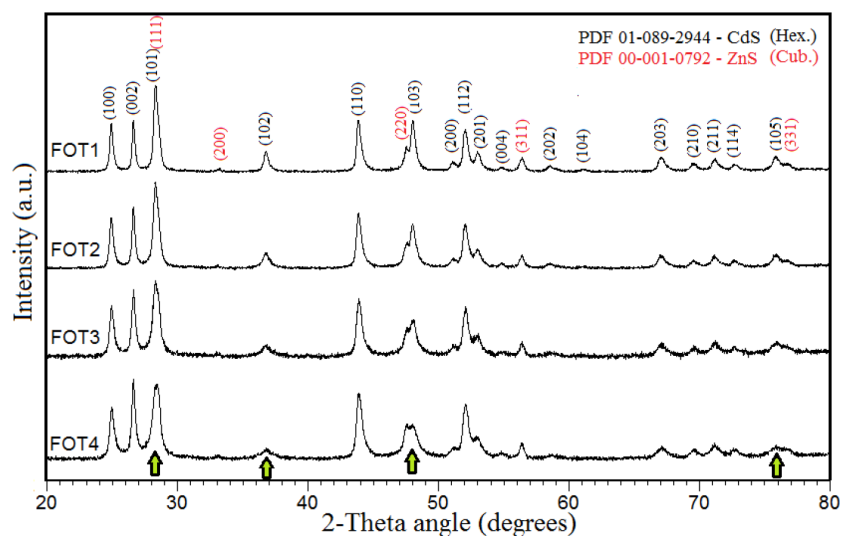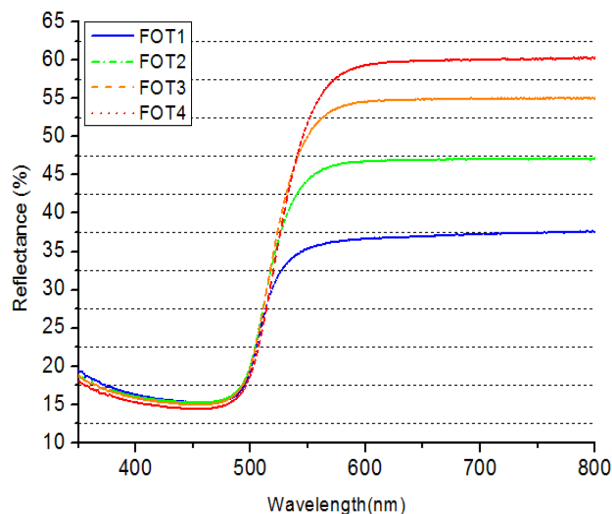
Figure 1. XRD spectra of FOT1–FOT4 samples.

Figure 2. Diffuse reflectance spectra for different photocatalysts.

the linear part of this dependency until the abscise intersection. The determined Eg value was the same for all photocatalysts, being 2.41 $\pm$ 0.05 eV, a value close to that of the pure CdS compound.[23] The DSR spectra highlight the decrease in the diffuse reflectance value at 750 nm wavelength along with the increase in cocatalyst charging, from about 60% for a 0.11% degree of PdS charging to 37% for a 0.86% degree of PdS charging, as shown in Figure 2. At a 750 nm wavelength the only absorbent compound is PdS with a band gap value of about 1.56 eV.[24] Light absorbance by the PdS lowers the photon flux, which can lead to electron-hole pairs that are useful for the photocatalytic process.

The UV-vis DRS results show that the absorption edge of CdS is not shifted after PdS loading but the absorption level is enhanced, especially in the visible light region after 600 nm. High change in the light absorption was observed, indicating that PdS was deposited on the surface of CdS instead of doping into the CdS lattice.
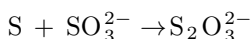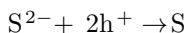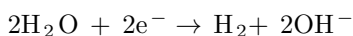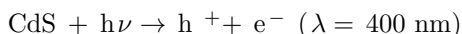
From the TEM images, as shown in Figure 3a, it can be observed that there are two types of regular shape crystals, having hexagonal morphology, and others at smaller sizes with irregular shapes. In order to achieve a more accurate measurement of the interplanar distances, in HR-TEM images, as shown in Figure 3b, the distance between 10 atomic planes was measured. Therefore, the measured interplanar distance is 3.16 Å, which, in the XRD spectrum, corresponds to a 100% relative intensity, with a Miller index of (101); the second one is 2.45 Å, corresponding to the relative intensity maximum of 25% and with a (102) Miller index. CdS crystallisation, having a different orientation on the CdS germs formed in the first stage, leads to the formation of macles as observed in Figure 3c.

EDX maps, as shown in Figures 3d–3f, highlight clearly that the hexagonal crystallised formations are CdS, the other ones being ZnS single crystals decorated with PdS. Therefore, the zinc sulphide acts like a palladium source, a part of the cocatalyst crystallising on the cubic ZnS surface, as shown in the r1 chemical reaction. On the surface of the hexagonal crystals often the existence of cocatalyst particles can be observed, making CdS doping possible with small Pd^{2+} quantities from this compound solubilisation during the hydrothermal process. The slow release of S^{2-} ions in the system, due to the low ZnS solubility allows the CdS slow growth, which leads to the obtaining of large size crystals (tens to hundreds nm) as we said before.

The EDX spectra, as shown in Figure 4a, are highlighting only the Cd, Zn, and S presence, confirming the purity of the ZnS–CdS mixture, which is in agreement with the XRD spectra. Small quantities of Pd^{2+} from the sample (under 0.7%) and the fact that the EDX maxima of palladium are "covered" by those of cadmium, do not allow the identification of this element in the EDX spectra.

As shown in Figure 4b, the Cd/Zn molar ratio in photocatalyst decreases with the palladium loading increase. Due to the fact that the palladium loading is performed initially on ZnS nanoparticles, the formation of PdS/ZnS-type core-shell nanoparticles is possible at room temperature. The ZnS surface, covered initially with PdS by the ion exchange process, as shown in reaction r1, increases with the $PdCl_2$ quantity increase that is added to the ZnS suspension. PdS, having a much lower solubility than ZnS, might partially block the hydrothermal ZnS solubilisation, according to reaction r2. This explains the higher ZnS content in the FOT1 photocatalyst compared to FOT3 and FOT4.

During the photocatalytic process the following reactions occur:

$CdS + h\nu \rightarrow h^+ + e^-$ ($\lambda = 400$ nm)

$2H_2O + 2e^- \rightarrow H_2 + 2OH^-$

$S^{2-} + 2h^+ \rightarrow S$

$S + SO_3^{2-} \rightarrow S_2O_3^{2-}$

During the photocatalytic process all photocatalysts exhibit a high degree of stability, not showing any deactivation after 20 h of photocatalysis as shown in Figure 5a. The rate of hydrogen evolution has an almost linear rise with the increase in PdS content in the photocatalyst. Thus the speed of hydrogen evolution increases by only 79% at an 8 times higher PdS concentration as shown in Figure 5b. At the same time, the reflectance at a 750 nm wavelength drops with 62%. Therefore, the speed limitative process in the hydrogen evolution reaction is not the recombination process but the density of the active centres for the reaction of hydronium ions reduction. The main advantage of the deposited photocatalyst on polymeric tapes is that stirring is not necessary to maintain the photocatalyst in suspension. Among the disadvantages of the photocatalyst deposited on supports we can name the high cost and the fact that part of the photocatalyst surface is in contact with the polymeric support, becoming inactive for the photocatalysis reaction.
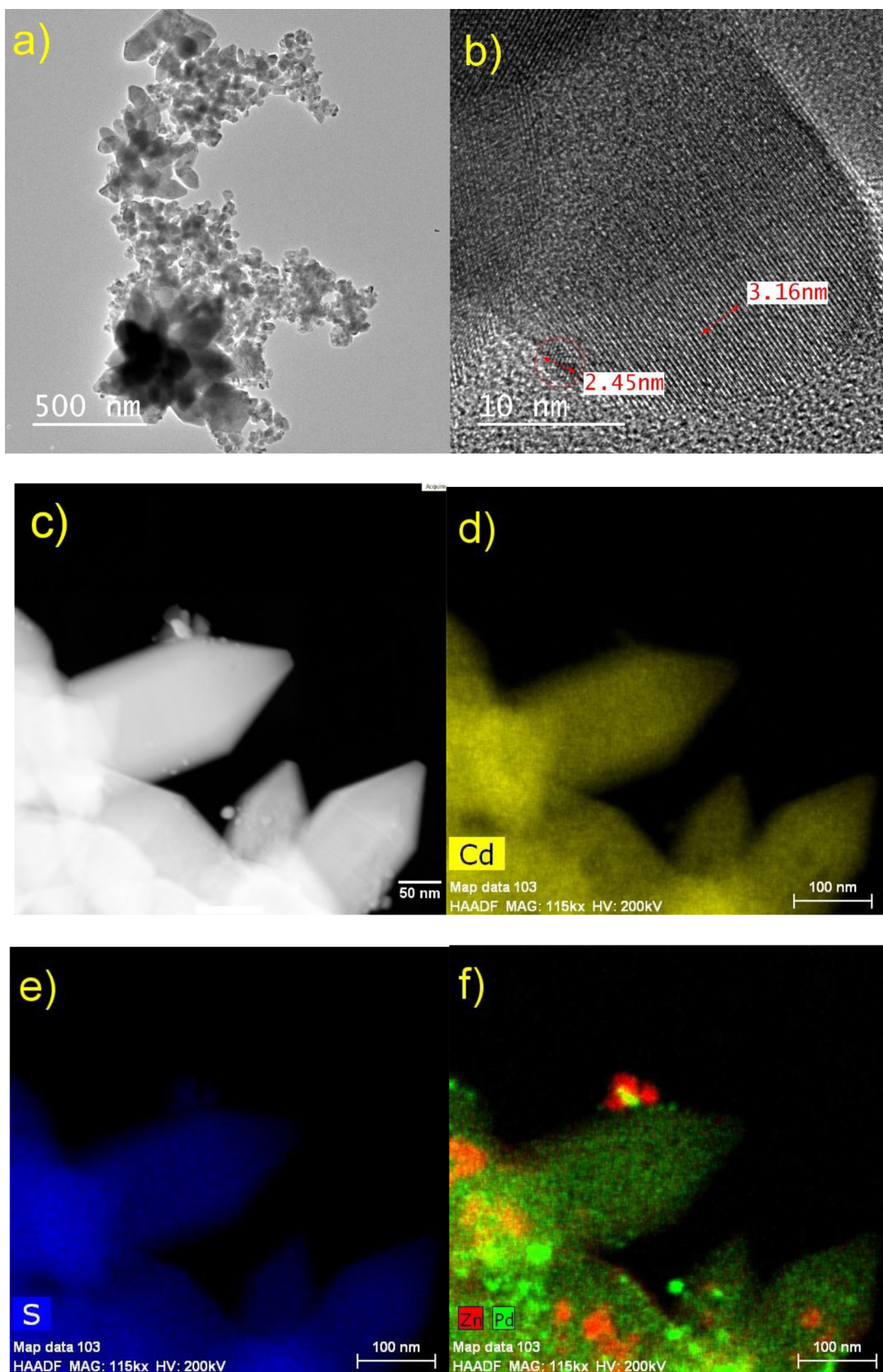
Figure 3. TEM (a), HR-TEM (b), STEM (c), and EDX mapping (d–f) of the FOT1 compound.
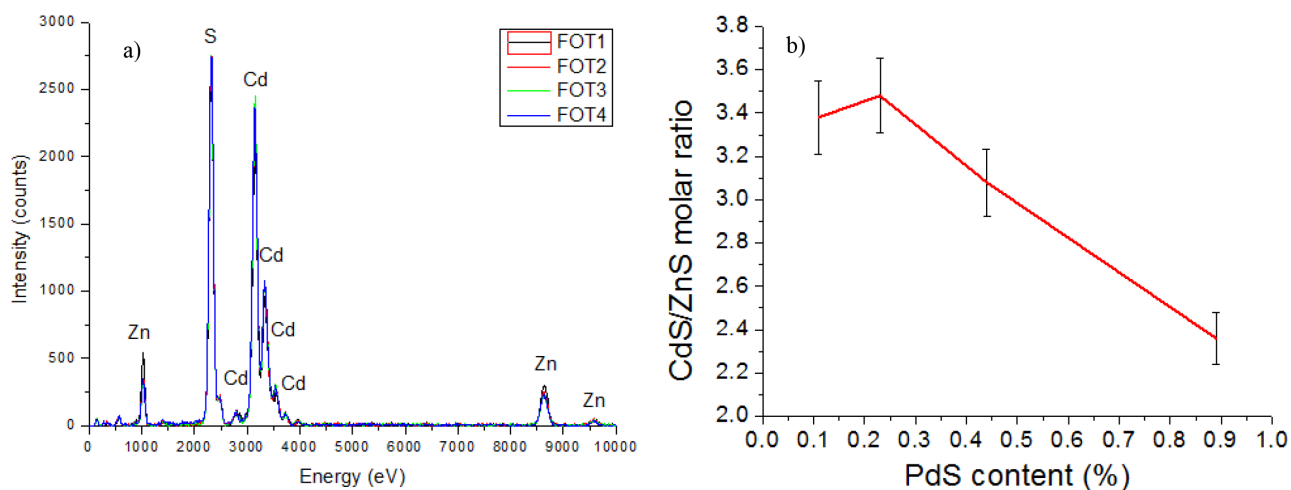
Figure 4. EDX spectra of FOT1–FOT4 photocatalysts, normalised at K line of sulphur (a) and the Cd/Zn molar ratio variation accordingly to the PdS loading of the photocatalyst (b).

In the case of the suspension photocatalyst, the experimental set-up is rigorously identical in all cases. Figures 5c and 5d illustrate the photoreactor with the photocatalyst loaded on polymeric support, before and during the illumination. Under blue light the hydrogen bubbles can be observed.

For the FOT1 photocatalyst deposited on magnetic support, the determined photocatalytic efficiency was 20 μmols/cm^2 h (Figure 5e); however, this value is strongly influenced by the support position towards the light source and the loading of the support with photocatalyst, which can lead to errors.

Figure 5e shows that the activity of the deposited photocatalyst decreases after 2 h of illumination. This effect is probably due to the photocatalyst photocorrosion in the conditions of increased irradiation expressed as mJ/cm^2 photoactive surface.

After deactivation, the photocatalyst deposited on polymeric bands may be dissolved with the aid of a strong acid (sulphuric and nitric acid). The polymeric bands can be thus reused. In order to optimise the photocatalytic process supplementary studies are necessary for the determination of the optimum irradiation in which the photocorrosion process has a minimum value.

In conclusion, CdS and ZnS mixture-based photocatalysts decorated with PdS in different concentrations were synthesised and characterised. It was observed, in all cases, that the photocatalysts' efficiency in the water splitting reaction increases with the increase in PdS loading even when the ZnS quantity in the photocatalyst increases and PdS screens the photoactive particles. Polymeric magnetic bands were manufactured and covered with photocatalyst. Due to the spatial separation of the magnetic/PMMA nanoparticles from the photocatalyst, the recycling process can be much simpler, the sulphides being able to be dissolved with the aid of a strong acid without the necessity of iron to cadmium and zinc separation. The magnetic bands can be maintained in the required position in the solution without the aid of stirring for maintaining the photocatalyst in suspension.

3. Experimental

3.1. Zinc sulphide synthesis

In the first stage ZnS was precipitated by adding Na$_2$S (Sigma Aldrich) to a ZnSO$_4$ (Chimreactiv) solution; then the obtained precipitate was crystallised hydrothermally at 200 °C for 20 h. The crystallised precipitate
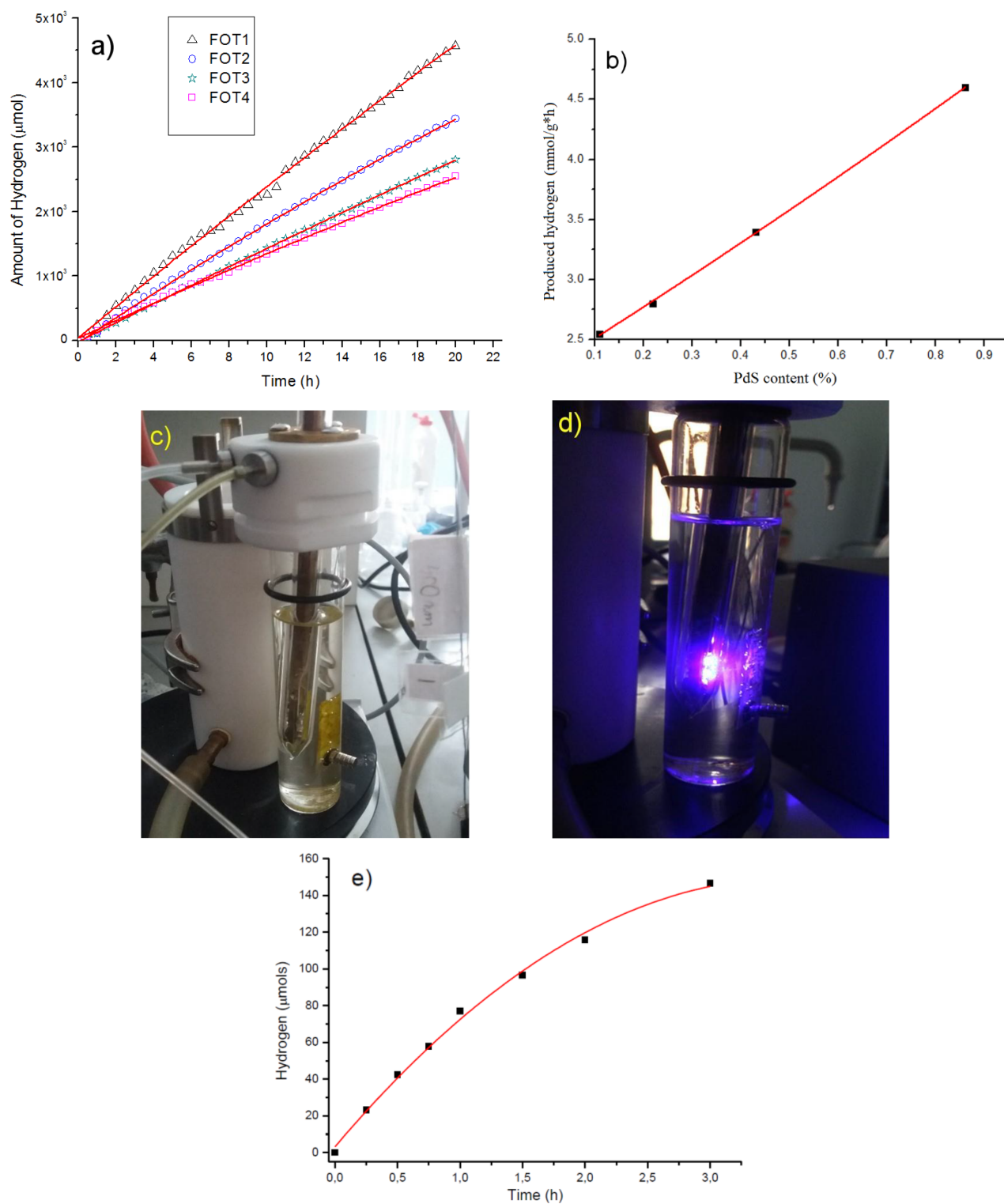
Figure 5. Hydrogen evolution curves for FOT1–FOT4 photocatalysts in suspension (a), the hydrogen quantity unloaded from the photocatalyst depending on the PdS loading of the photocatalyst (b), photographs of photocatalysts deposited on polymeric bands loaded with photocatalysts in a 0.35 M S^{2-} and 0.25 M SO_3^{2-} solution placed before (c) and during (d) blue light illumination, (e) hydrogen evolution curves for FOT1 photocatalyst deposited on PP bands.

was separated by filtration, then washed with water, and dried in a vacuum at 60 °C. The extended version of this synthesis is described in our previous paper.[17]

3.2. Photocatalysts synthesis

First 585 mg of ZnS was suspended as in the method described before in 30 mL of water under sonication for 30 min. After this, 2 mL of glacial acetic acid was added under stirring. After 5 min, 16 mL of $PdCl_2$ (Sigma Aldrich) solution with 0.64 mg/mL concentration was added. The immediate change in suspension colour from white to brown indicated that the reaction between Pd^{2+} and ZnS, with the formation of the PdS low solubility compound, took place according to reaction r1. After 2 min of suspension homogenisation, 1070 mg of cadmium acetate dihydrate (Sigma Aldrich) was added. The mixture was transferred to an autoclave with PTFE liner. The autoclave was placed in an oven at 200 °C for 72 h. Afterwards the autoclaves were cooled naturally at room temperature. The photocatalyst was filtrated, washed with water and the last time with ethanol, and dried under vacuum at 60 °C. The sample was named FOT1. In a similar way FOT2, FOT3, and FOT4 photocatalysts were prepared adding to the ZnS suspension 8, 4, and 2 mL of $PdCl_2$ solution.

3.3. Polymer mounts' manufacturing and photocatalyst loading

On PP/adhesive (Self-laminating Cards, 3L Office Products) polymer mounts having dimensions of about 15×40 mm was placed drop by drop, with intermediary drying between drops, 100 μ L of nanoparticles suspension of newly prepared magnetite (by coprecipitation of Fe^{2+} and Fe^{3+} ions with NH_4OH), dispersed in a 5% polymethyl methacrylate in chloroform solution. The photocatalyst loading was achieved by pressing the polymeric mount with the adhesive part on the FOT1 photocatalyst powder.

3.4. Photocatalysis experiments

First 40 mL of aqueous solution of 0.35 M sodium sulphide (Sigma Aldrich) and 0.25 M sodium sulphite (Sigma Aldrich) was prepared. In this solution, 50.0 mg of photocatalyst was dispersed in the experiments that used dispersed photocatalyst and polymeric bands loaded with photocatalyst in the experiments with supported photocatalyst. The suspension was sonicated under vacuum for 5 min and then the photoreactor was filled with nitrogen. It was lit with 400 nm wavelength light. As the light source two LED diodes OF-SMD3535UV type powered by 3.1 V and 0.45 A were used. The gas was identified by gas chromatography as being pure hydrogen and measured quantitatively by the volumetric method.

3.5. Characterisation

The obtained powders were characterised by X-ray diffraction (X'Pert PRO MPD PANalytical diffractometer, CuKα radiation, $\lambda = 1.54184$ Å), UV-Vis spectroscopy (Lambda 950, PerkinElmer), scanning electron microscopy (Inspect S FEI), and transmission electron microscopy (Titan G2 80-200 FEI).

References

1. Koca, A.; Sahin, M. *J. Chem. Edu.* **2003**, *80*, 1314-1325.

2. Li, G. S.; Zhang, D. Q.; Yu, J. C. *Environ. Sci. Technol.* **2009**, *43*, 7079-7085.

3. Ashokkumar, M. *Int. J. Hydrogen Energy* **1998**, *23*, 427-438.

4. Kudo, A. *Int. J. Hydrogen Energy* **2006**, *31*, 197-202.

5. Maeda, K.; Teramura, K.; Lu, D.; Takata, T.; Saito, N.; Inoue, Y.; Domen, K. *Nature* **2006**, *440*, 295-295.

6. Deshpande, A.; Shah, P.; Gholap, R. S.; Gupta, N. M. *J. Colloid Interf. Sci.* **2009**, *333*, 263-268.

7. Zhang, J. L.; Xiao, M.; Liu, Z. M. *J. Colloid Interf. Sci.* **2004**, *273*, 160-164.

8. Liu, S.; Li, H.; Yan, L. *Mater. Res. Bull.* **2013**, *48*, 3328-3334.

9. Jing, D.; Guo, L.; Zhao, L.; Zhang, X.; Liu, H.; Li, M.; Shen, S.; Liu, G.; Hu, X.; Zhang, X.; et al. *Int. J. Hydrogen Energy* **2010**, *35*, 7087-7097.

10. Xing, C.; Zhang, Y.; Yan, W.; Guo, L. *Int. J. Hydrogen Energy* **2006**, *31*, 2018-2024.

11. Li, Y.; Du, J.; Peng, S.; Xie, D.; Lu, G.; Li, S. *Int. J. Hydrogen Energy* **2008**, *33*, 2007-2013.

12. Wang, Q.; Li, J.; Bai, Y.; Lian, J.; Huang, H.; Li, Z.; Lei, Z.; Shangguan, W. *Green Chem.* **2014**, *16*, 2728-2735.

13. Wang, X.; Liu, G.; Lu, G. Q.; Cheng, H. M. *Int. J. Hydrogen Energy* **2010**, *35*, 8199-8205.

14. Sathish, M.; Viswanathan, B.; Viswanath, R. P. *Int. J. Hydrogen Energy* **2006**, 31, 891-898.

15. Yan, H.; Yanga, J.; Ma, G.; Wu, G.; Zonga, X.; Lei, Z.; Shi, J.; Li, C. *J. Catal.* **2009**, *266*, 165-168.

16. Sasikala, R.; Gaikwad, A. P.; Sudarsan, V.; Rao, R.; Jagannath; Viswanad, B.; Bharadwaj, S. R. *Phys. Chem. Chem. Phys.* **2015**, *17*, 6896-6904.

17. Svera, P.; Racu, A. V.; Mosoarca, C.; Ursu, D.; Linul, P. A.; Băies, R.; Bănică, R. *J. Optoelectron. Adv. M.* **2016**, *18*, 1027-1032.

18. Yang, J.; Yan, H.; Zong, X.; Wen, F.; Liu, M.; Li, C. *Philos. Trans. A Math. Phys. Eng. Sci.* **2013**, *371*, 20110430.

19. Zhang, Y. J.; Zhang, L. *Appl. Surf. Sci.* **2009**, *255*, 4863-4866.

20. Rufus, I. B.; Ramakrishnan, V.; Viswanathan B.; Kuriacose J. C. *Langmuir* **1990**, *6*, 565-567.

21. Hasegawa, M.; Iyoda, M. *Chem. Soc. Rev.* **2010**, *39*, 2420-2427.

22. Pan, P.; Wood, S. A. *Miner. Deposita.* **1994**, *29*, 373-390.

23. Pan, H. *Renew. Sust. Energ. Rev.* **2016**, *57*, 584-601.

24. Ehsan, M. A.; Ming, H. N.; McKee, V.; Anton, T.; Peiris, N.; Gamage, W. K. U.; Arifin, Z.; Mazhar, M. *New J. Chem.* **2014**, *38*, 4083-4091.